

Nonlocal cable-network metamaterials

Yi Chen^{}, Mahmoud A. A. Abouelatta, Ke Wang Muamer Kadic and Martin Wegener^{*}*

Y. Chen, M. Wegener

Institute of Nanotechnology, Karlsruhe Institute of Technology (KIT), Karlsruhe 76128, Germany.

Y. Chen, M. A. A. Abouelatta, K. Wang, M. Wegener

Institute of Applied Physics, Karlsruhe Institute of Technology (KIT), Karlsruhe 76128, Germany.

K. Wang

Center for Composite Materials, Harbin Institute of Technology (HIT), Harbin 150001, China.

M. Kadic

Institut FEMTO-ST, UMR 6174, CNRS, Université de Bourgogne Franche-Comté (UBFC), Besançon 25030, France.

E-mail: (yi.chen@partner.kit.edu (Y.C.); martin.wegener@kit.edu (M.W.))

Keywords: metamaterials, cable-network, nonlocal interactions, dispersions relations

Abstract: Metamaterials are artificial materials in which the atoms of ordinary solids are replaced by tailored functional building blocks. Therefore, previous work has emphasized tailoring the inside of the building blocks, for example by exploiting local resonances, to realize unusual effective metamaterial properties. However, the wave properties of a metamaterial are not only determined by its building blocks but also by the interactions between these building

blocks. Here, reconfigurable “plug-and-play” electromagnetic metamaterials are introduced for which the building blocks are essentially trivial standard BNC connectors and the effective metamaterial properties are solely achieved by tailoring the local and especially the nonlocal interactions mediated by standard coaxial cables. Unprecedented dispersion relations of the lowest band with multiple regions of slow waves and backward waves are demonstrated. Importantly, the dispersion relation of such metamaterials dominated by nonlocal interactions is not limited by the principle of causality in the same way as for metamaterials designed by local resonances of building blocks.

1. Introduction

In metamaterials, the atoms of ordinary materials are replaced by designed functional building blocks that can be arranged periodically in analogy to atoms in a crystal. In addition, the building blocks clearly need to be connected by some sort of interaction to support wave propagation. Designing local resonances of the building blocks combined with simple interactions has led to a large variety of optical,^[1,2] mechanical,^[3,4] and acoustical metamaterials^[5,6] with interesting wave properties, which can be expressed by the wave's dispersion relation $\omega(k)$, i.e., by the dependence of the wave's angular frequency ω versus its wavenumber k . However, whatever the specific design may be, the frequency dependence of the metamaterial's response function must obey causality, i.e., an action at time t_0 only leads to reactions at future times $t > t_0$. Mathematically, causality leads to fundamental restrictions of the real and imaginary parts of the response function via the Kramers-Kronig relations.^[7] These restrictions concern the possible bandwidth of targeted effective properties and the connection to unavoidable losses or damping in the vicinity of the local resonances. These restrictions have, for example, been discussed in great detail for the case of metamaterials with negative^[8-10] and zero^[11,12] effective refractive index.

Here, we follow the polar opposite design paradigm for tailoring the dispersion relation $\omega(k)$ of electromagnetic metamaterials for the lowest band. We consider essentially trivial and conceptually point-like building blocks (BNC cable connectors) without any resonances in the relevant frequency regime and rather design the metamaterial dispersion relation by tailoring the local and nonlocal interactions among these building blocks in real space by using coaxial cables with designed cable lengths between nodes. In Fourier space this means that we tailor the effective wavenumber dependence ("spatial dispersion") of the metamaterial response function rather than its frequency dependence directly. We nickname such reconfigurable "plug-and-play" metamaterials based on networks of coaxial cables cable-network metamaterials.

Nonlocality in electromagnetism^[13-19] is distinct from Bragg resonances as, e.g., used in photonic crystals.^[20] Our present builds on networks of waveguides exhibiting spatial dispersion in electromagnetism^[21,22] and acoustics.^[23,24] Networks of coaxial cables as waveguides have recently been used in the context of non-Abelian topological charges and edge states in metamaterials.^[25] Why coaxial cables? In our design approach, one first needs to decide on how to realize the local and nonlocal interactions among the conceptually point-like building blocks of the metamaterial. At first sight, any waveguide appears suitable. However, we ideally want the waveguide to be loss-free and broadband. In particular, we do not want any cut-off

frequency of the waveguide as this would, from the start, prohibit tailoring of the dispersion relation from zero frequency upwards. Furthermore, it is highly desirable that the waveguide supports only a single mode over the entire bandwidth. Otherwise, a waveguide of a certain length l supporting a certain number of modes would represent not just a single fixed interaction but rather an interaction that depends on how the incident field exactly couples into the waveguide. A possible choice for the waveguides are standard coaxial cables (see **Figure 1**) with a wave impedance of 50Ω and a wave speed of about $2/3$ of the vacuum speed of light from zero frequency to some Gigahertz.^[26] Wave propagation losses are typically as low as some 0.01 dB/m .^[26] The electric field of the single propagating mode is radially polarized and is concentrated to the region between the two concentric cylindrical metallic conductors. This region is typically filled with a dielectric, serving as a spacer and holder. Conceptually, this region could be filled by vacuum. If the metal acts like a perfect electric conductor, the properties of this coaxial waveguide would be strictly frequency independent in the considered regime. Nevertheless, the finite wave speed means that the interaction mediated by a coaxial cable must obey the principle of causality, leading to a generalized form of the Kramers-Kronig relations^[27,28] for frequency- and wavenumber-dependent response functions.

2. Dispersion bands of nonlocal cable-network metamaterials

Figure 1 schematically illustrates an example of a cable-network metamaterial built from coaxial cables and BNC connectors. For simplicity, we depict an arrangement that is periodic along only the x -direction, with period or lattice constant a . Cables with length l_1 connect the nearest-neighbor connection points, cables with length l_N connect N -th ($N = 2, 3, \dots$) nearest neighbors. We have obtained (for derivation see Supporting Information Note 1) the dispersion relation $\omega_i(k)$ ($i = 1, 2, \dots$) of the cable network metamaterial by considering its Bloch periodicity and Kirchhoff's law of current continuity at the connection nodes from the analytical implicit equation

$$\frac{\cos(Nka) - \cos\left(\omega_i \frac{l_N}{c_N}\right)}{Z_N \sin\left(\omega_i \frac{l_N}{c_N}\right)} + \frac{\cos(ka) - \cos\left(\omega_i \frac{l_1}{c_1}\right)}{Z_1 \sin\left(\omega_i \frac{l_1}{c_1}\right)} = 0. \quad (1)$$

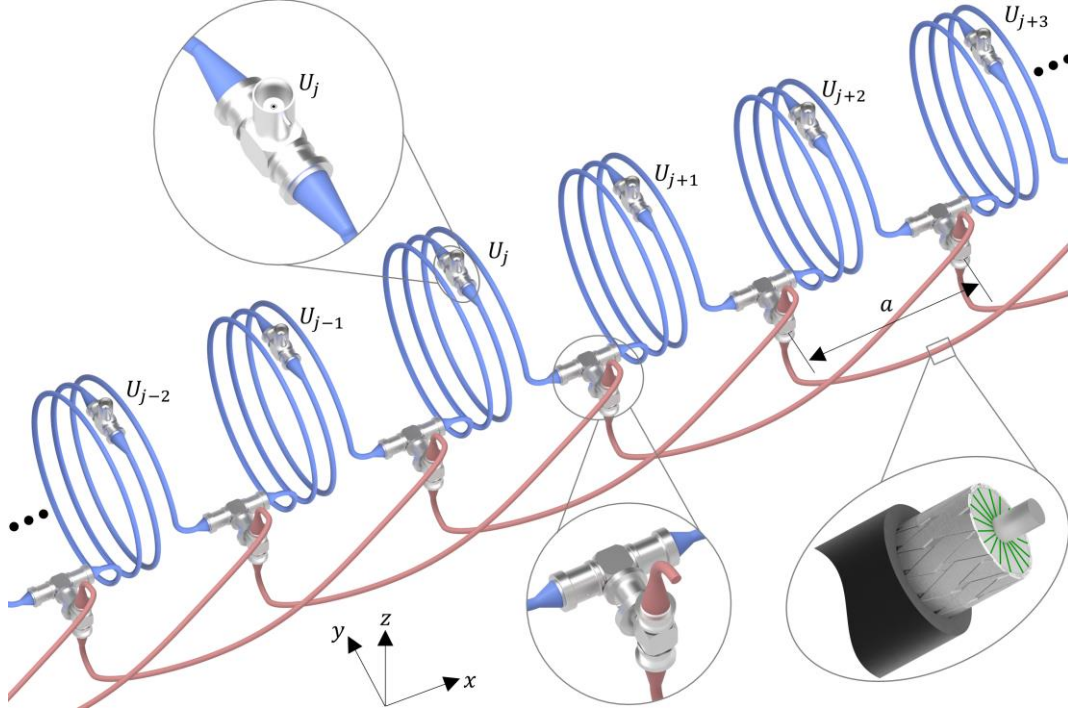


Figure 1. Illustration of a metamaterial composed of a network of coaxial cables. Rendered scheme of a one-dimensional periodic arrangement of building blocks (BNC connectors) with period a along the x -direction. Adjacent building blocks are connected by coaxial cables of length l_1 (local connections, blue). In addition, the N -th nearest neighbors are connected by coaxial cables of length l_N (nonlocal connections, red). The case of $N = 2$ is shown as an example. Note that the geometrical arrangement of the cables within one unit cell is irrelevant. It is only the ratio l_1/l_N and the order of nonlocal interaction N which determine the shape of the dispersion relation of the waves propagating along the x -direction within the metamaterial (see Figure 2 and 3). One inset is a magnified view onto one BNC connector. The other inset shows an oblique view onto a cut single coaxial cable composed of two concentric metal cylinders (gray) and its radially polarized electric-field lines (green). The coaxial cable is one example for a frequency independent broadband low-loss single-mode electromagnetic waveguide.

Causality, which demands that an action on one end of a cable at one point in time leads to a time delayed future response at the other end that is compatible with the theory of relativity, is fulfilled via the finite cable wave speeds c_1 and c_N . Clearly, the lattice constant a merely scales the wavenumber axis k . For identical cables, the impedances are equal, $Z_1 = Z_N = Z$, and drop out. We further have $c_1 = c_N = c$. The choice of c merely scales the frequency axis. The cable length l_1 scales the frequency axis as well, such that only the dimensionless cable-length ratio l_1/l_N effectively determines the qualitative shape of the band structure. In general, the band structure contains one lowest “acoustical” ($i = 1$) branch and many “optical” ($i = 2, 3, \dots$) branches because a cable has more than one degree of freedom as the instantaneous

voltage along the cable axis is not necessarily constant. **Figure 2** shows calculated band structures for the examples of $N = 2$ (top row), $N = 4$ (middle row), and $N = 6$ (bottom row). The columns of the resulting “matrix” of panels in Figure 2 correspond to different ratios l_1/l_N as indicated.

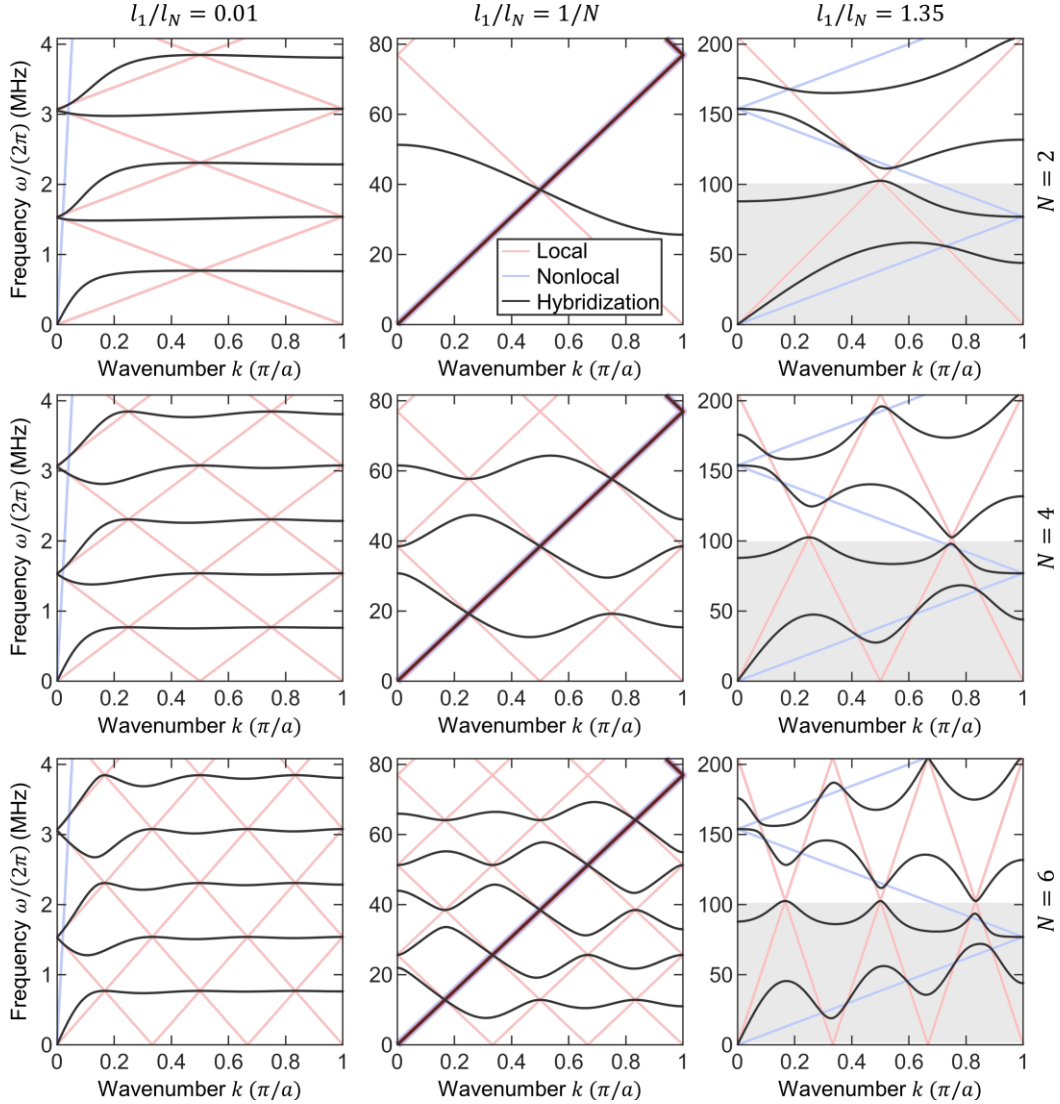


Figure 2. Calculated band structures of the cable-network metamaterial. We consider the dispersion relation $\omega_i(k) = \omega_i(-k)$, with integer band index $i = 1, 2, \dots$, of the cable-network metamaterial composed of nearest-neighbor and N -th nearest-neighbor interactions (cf. Figure 1). The integer N and the cable-length ratio l_1/l_N determine the shape of the dispersion relation. The subpanels of this figure are arranged in form of a matrix. The three rows of this matrix correspond to $N = 2$, $N = 4$, and $N = 6$. The three columns of this matrix correspond to the ratios $l_1/l_N = 0.01$, $1/N$, and 1.35 , respectively, at fixed $l_1 = 130$ cm. For $l_1/l_N = 1.35$ (cf. Figure 3), the lowest band $\omega_1(k)$ exhibits multiple regions of slow and negative group velocity, equivalent to a negative refractive index for negligible losses. The band structure of the cable network $\omega_i(k)$ (black curves) results from a hybridization of the “bare” dispersion relations of

having only the local cables (blue curves) and those of having only the nonlocal cables (red curves).

To obtain an intuitive understanding, we compare the dispersion relation of the nonlocal cable-network metamaterial with the “bare” dispersion relation for having only the local cables and that of having only the nonlocal cables. These are given by $\omega = v_1 k$ with wave speed $v_1 = ca/l_1$, and $\omega = v_N k$ with wave speed $v_N = cNa/l_N$, respectively. Both are slowed down with respect to a straight cable ($\omega = ck$) due to the geometrical detour of the cables (cf. Figure 1, also Figure S1) with respect to a straight connection between the connectors, analogous to the slowing down in labyrinthine metamaterials.^[29] For the particular case of $l_1/l_N = 1/N$, the two bare wave speeds are identical, $v_1 = v_N$. For all panels in Figure 2, we plot the bare local dispersion relation in blue and that of the bare nonlocal dispersion in red within the first Brillouin zone with $|k| \leq \pi/a$. For the bare nonlocal dispersion relation (for which the first Brillouin zone is smaller and given by $|k| \leq \pi/(Na)$), we can add/subtract reciprocal lattice vectors according to $k \rightarrow \pm m 2\pi/(Na)$ with integer m . In each of the cases depicted in Figure 2, the dispersion relation of the cable network (black curves) is a hybridization of these bare dispersion relations. In the limit of long nonlocal cables, $l_1/l_N \ll 1$, a stop band evolves, similar to a photonic crystal^[20] or the hybridization of a local resonance with a propagating mode.^[3] In the special case of $l_1/l_N = 1/N$, the first and the second band cross. In the most interesting case of short nonlocal cables, $l_1/l_N > 1$ (to be used in the below experiments), the first and the second band exhibit a pronounced avoided crossing, leading to multiple maxima and minima of the lowest band $\omega_1(k)$ versus k , with regions of negative group velocity $v_{\text{group}} = d\omega/dk$ in between. The effect of nonzero cable propagation losses is discussed in the Supporting Information (see Supporting Information Note 2 and Figure S2).

3. Experiment results

In our experiments, we choose $a = 5$ cm, $l_1 = 130$ cm = $26 \times a$, $l_N = 96$ cm, hence $l_1/l_N = 1.35$, and a total of 40 metamaterial unit cells, i.e., the total metamaterial length is $40 \times a = 2$ m. Different values of N can simply be obtained by rearranging the cables in a “plug-and-play” manner. Different interaction strengths could be realized by different cable lengths. Photographs of the setup are shown in Figure S3 and S4. We excite the cable-network metamaterial by a sinusoidal voltage signal with about 1 V amplitude at angular frequency ω from a function generator (Keysight, 33600A) connected to the left-hand side end of the metamaterial. The right-hand side end is terminated by a 50 Ω resistor, which is impedance-matched to the 50 Ω coaxial cables. The T-connectors in the nearest-neighbor cables at the top

allow us to measure the voltage $U_j(t)$ ($j = 1, 2, \dots, 40$) at a point in each metamaterial unit cell by means of a fast digital oscilloscope (Siglent, SDS5054X). We use an identical 10 cm short BNC cable to connect to the oscilloscope for all unit cells (i.e., the oscilloscope needs to be moved for the different j). The oscilloscope is independently triggered by the function generator. The complex-valued Fourier components, $\tilde{A}_j(\omega)$, at frequency ω , is extracted from $U_j(t)$. Fourier transformation of the $\tilde{A}_j(\omega)$ with respect to the real-space position $x = ja$ yields the wavenumber k . The resulting modulus of the measured amplitude $|\tilde{A}(\omega, k)|$ provides us with the metamaterial electromagnetic band structure – just like the scattering amplitude in inelastic neutron scattering on ordinary solids provides one with the phonon band structure.

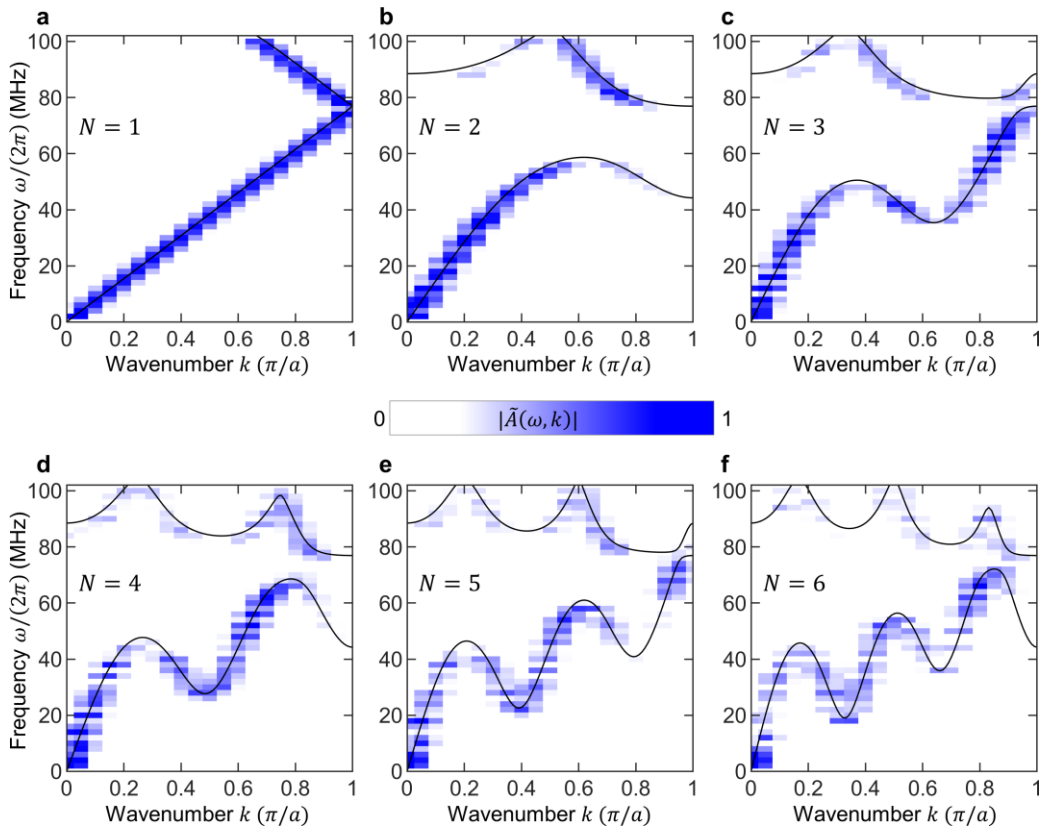


Figure 3. Measured cable-network metamaterial dispersion relations. The amplitudes $|\tilde{A}(\omega, +k)| \equiv |\tilde{A}(\omega, -k)|$ shown on a normalized false-color scale are obtained from a double Fourier transform of the measured voltage signals $U_j(t)$ at the spatial positions $x = ja$ with $j = 1, \dots, 40$ on a metamaterial (cf. Figure 1) with 40 unit cells. The underlying raw data are depicted in Figure S5. Shown in the six panels are the six examples of $N = 1, 2, 3, 4, 5,$ and 6 . The black solid curves are the band structures calculated for an infinitely periodic and lossless metamaterial (see Figure 1) for the same parameters as in Figure 2.

Experimental results for $N = 1, 2, 3, 4, 5,$ and 6 are shown in **Figure 3**. Herein, the amplitude $|\tilde{A}(\omega, k)|$ extracted from the experiment is shown on a false-color scale. Only

positive wavenumbers are shown due to the symmetry $|\tilde{A}(\omega, +k)| \equiv |\tilde{A}(\omega, -k)|$. Frequency $\omega/(2\pi)$ has been varied in equidistant steps of 2 MHz. The 40 steps in wavenumber with step width $\Delta k = 2\pi/(40 \times a)$ immediately result from the finite number of 40 metamaterial unit cells. The additionally shown gray curves are the band structures obtained from the above implicit analytical formula for the cable-network metamaterial for infinitely many unit cells and for zero losses. Herein, the cable lengths are directly taken from the experiment and include the lengths added to the coaxial cables by the BNC cable connectors. Obviously, the overall agreement between theory and experiment is excellent, even for the extremely complex dispersion relation of the lowest band for $N = 6$, for which we find three maxima and three minima of $\omega_1(k)$ versus k within the first Brillouin zone with $|k| \leq \pi/a$.

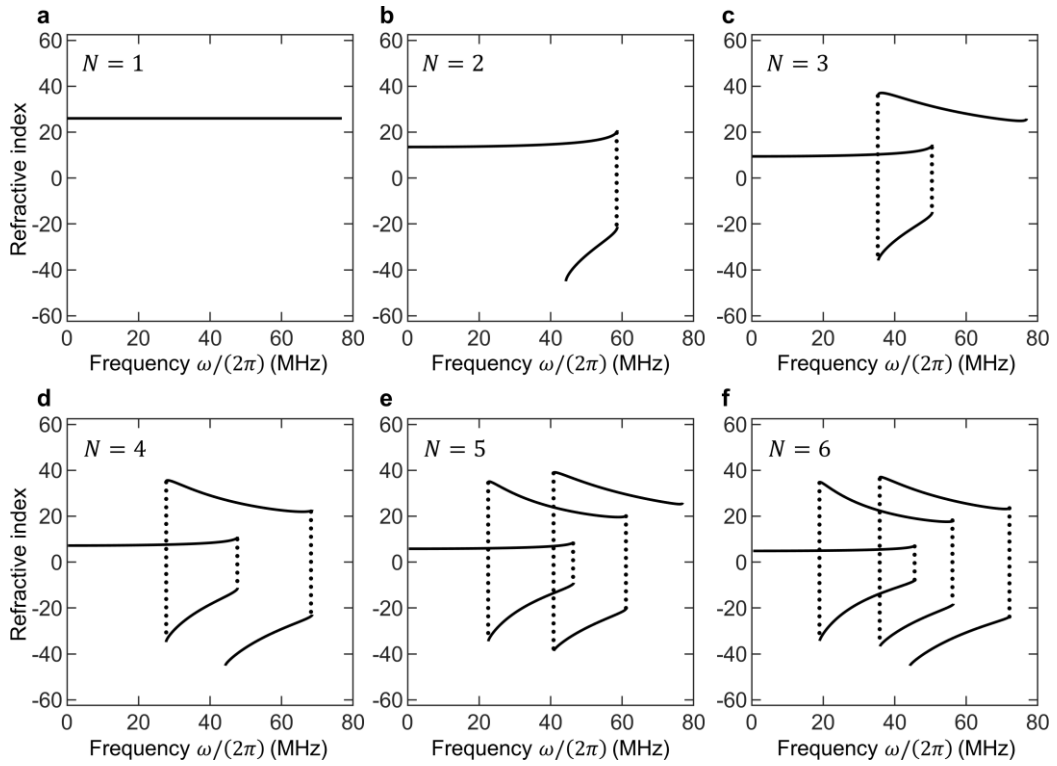


Figure 4. Effective metamaterial refractive indices. The refractive-index spectra $n(\omega) = \tilde{n}(k(\omega))$ are deduced from the six data sets shown in Figure 3. At many frequencies ω , modes with positive and negative refractive index coexist.

Finally, from the calculated or measured dispersion relations of the lowest band $\omega_1(k)$, we can immediately infer the effective refractive index $n(\omega) = \tilde{n}(k(\omega))$ (see Supporting Information Note 3). The result shown in **Figure 4** for the same examples as in Figure 3 is multi-valued. In particular, it contains broad regions of negative refractive index, conceptually at zero loss, that have become possible due to using nonlocality for design and that would not be possible by using only local resonances, due to causality.

4. Conclusion

We have introduced periodic electromagnetic metamaterials based on networks of coaxial cables and standard BNC connectors as a reconfigurable plug-and-play platform to obtain unprecedented effective electromagnetic wave's dispersion relations of the lowest band by using nonlocality as a design tool. We emphasize that nonlocality is conceptually distinct from both, local resonances and Bragg reflections, which have previously been the main paths to artificial materials with interesting properties. Technologically, the presented system is extremely simple, such that it could well serve for educational purposes in university classes and schools. Scientifically, we foresee many possible future research avenues, including nonlocal interactions in higher spatial or synthetic dimensions, topological architectures, miniaturization towards optical frequencies, and hybrids of nonlocality and local resonances.

Supporting Information

Supporting Information is available from the Wiley Online Library or from the author.

Acknowledgements

We thank Filippo Capolino (Irvine, USA) and Changguo Wang (Harbin Institute of Technology, China) for discussions. Y.C. is grateful for support by the Alexander von Humboldt Foundation. This research has additionally been funded by the Deutsche Forschungsgemeinschaft (DFG, German Research Foundation) under Germany's Excellence Strategy via the Excellence Cluster "3D Matter Made to Order" (EXC-2082/1-390761711), which has also been supported by the Carl Zeiss Foundation through the "Carl-Zeiss-Foundation-Focus@HEiKA", by the State of Baden-Württemberg, and by the Karlsruhe Institute of Technology (KIT). We further acknowledge support by the Helmholtz program "Materials Systems Engineering" (MSE). M.K. is grateful for support by the EIPHI Graduate School (contract ANR-17-EURE-0002). K.W. acknowledges support by the China Scholarship Council (CSC). M.A.A.A. is grateful for support by the Erasmus Mundus Europhotonics M.Sc. Scholarship.

Received: ((will be filled in by the editorial staff))

Revised: ((will be filled in by the editorial staff))

Published online: ((will be filled in by the editorial staff))

Conflict of interests:

Authors declare that they have no competing interests.

Data and code availability:

The data that support the plots within this paper and other findings of this study are available from the corresponding authors upon reasonable request and are published on the open access data repository of the Karlsruhe Institute of Technology [Enter repository].

References

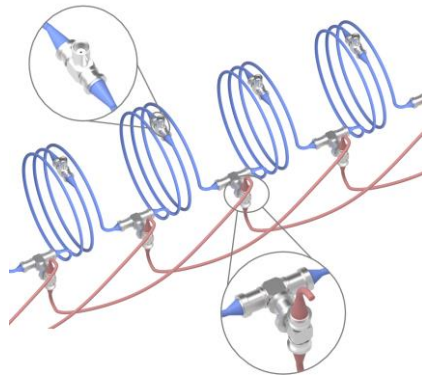
- [1] D. R. Smith, J. B. Pendry, M. Wiltshire, *Science* **2004**, 305, 788.
- [2] C. Soukoulis, S. Linden, M. Wegener, *Science* **2007**, 315, 1077.
- [3] Z. Liu, X. Zhang, Y. Mao, Y. Zhu, Z. Yang, C. T. Chan, P. Sheng, *Science* **2000**, 289, 1734.
- [4] K. Bertoldi, V. Vitelli, J. Christensen, M. Van Hecke, *Nat. Rev. Mater.* **2017**, 2, 1.
- [5] S. A. Cummer, J. Christensen, A. Alù, *Nat. Rev. Mater.* **2016**, 1, 1.
- [6] M. Kadic, G. W. Milton, M. van Hecke, M. Wegener, *Nat. Rev. Phys.* **2019**, 1, 198.
- [7] J. S. Toll, *Phys. Rev.* **1956**, 104, 1760.
- [8] M. I. Stockman, *Phys. Rev. Lett.* **2007**, 98, 177404.
- [9] T. G. Mackay, A. Lakhtakia, *Phys. Rev. Lett.* **2007**, 99, 189701.
- [10] D. Forcella, C. Prada, R. Carminati, *Phys. Rev. Lett.* **2017**, **118**, 134301.
- [11] M. H. Javani, M. I. Stockman, *Phys. Rev. Lett.* **2016**, **117**, 107404.
- [12] I. Liberal, N. Engheta, *Nat. Photonics* **2017**, **11**, 149.
- [13] P. A. Belov, R. Marques, S. I. Maslovski, I. S. Nefedov, M. Silveirinha, C. R. Simovski, S. A. Tretyakov, *Phys. Rev. B* **2003**, **67**, 113103.
- [14] C. Ciracì, R. T. Hill, J. J. Mock, Y. Urzhumov, A. I. Fernández-Domínguez, S. A. Maier, D. R. Smith, *Science* **2012**, 337, 1072.
- [15] N. A. Mortensen, S. Raza, M. Wubs, T. Søndergaard, S. I. Bozhevolnyi, *Nat. Commun.* **2014**, 5, 1.
- [16] J. B. Pendry, P. A. Huidobro, Y. Luo, E. Galiffi, *Science* **2017**, 358, 915.
- [17] R. Venkitakrishnan, T. Höß, T. Repän, F. Z. Goffi, M. Plum, C. Rockstuhl, *Phys. Rev. B* **2021**, 103, 195425.
- [18] S. Boroviks, Z. Lin, V. A. Zenin, M. Ziegler, A. Dellith, P. A. D. Gonçalves, C. Wolff, S. I. Bozhevolnyi, J. Huang & N. A. Mortensen, *Nat. Commun.* **2022**, 13, 1.
- [19] Z. Zhang, P. Delplace, R. Fleury, *Nature* **2021**, 598, 293.
- [20] J. D. Joannopoulos, P. R. Villeneuve, S. Fan, *Solid State Commun.* **1997**, 102, 165.
- [21] C. A. Moses, N. Engheta, *IEEE T. Antenn. Propag.* **1999**, 47, 918.

- [22] E. Feigenbaum, H. A. Atwater, *Phys. Rev. Lett.* **2010**, 104, 147402.
- [23] J. A. I. Martínez, M. F. Groß, Y. Chen, T. Frenzel, V. Laude, M. Kadic, M. Wegener, *Sci. Adv.* **2021**, 7, m2189.
- [24] Y. Chen, M. Kadic, M. Wegener, *Nat. Commun.* **2021**, 12, 1.
- [25] Q. Guo, T. Jiang, R. Zhang, L. Zhang, Z. Zhang, B. Yang, S. Zhang, C. T. Chan, *Nature* **2021**, 594, 195.
- [26] H. W. Silver, *The ARRL handbook: for radio communications*, AARL, Newington, USA **2011**.
- [27] J. G. Sun, A. Puri, *Opt. Commun.* **1989**, 70, 33.
- [28] S. A. R. Horsley, M. Artoni, G. C. La Rocca, *Nat. Photonics* 2015, 9, 436.
- [29] Z. X. Liang, J. Li, *Phys. Rev. Lett.* **2012**, 108, 114301.

A “plug-and-play” reconfigurable metamaterial platform based on standard coaxial cables and BNC connectors is proposed. Particularly, interesting nonlocal effects can be straightforwardly implemented through coupling unit cells in the metamaterial to their beyond-nearest-neighbors via coaxial cables. As examples, metamaterials with nonlocal interaction from 2rd order to 6th order are assembled and highly unusual dispersion relations from metamaterials with only local interactions are experimentally demonstrated.

Yi Chen*, Mahmoud A. A. Abouelatta, Ke Wang Muamer Kadic and Martin Wegener*

Nonlocal cable-network metamaterials



Supporting Information

Nonlocal cable-network metamaterials

Yi Chen^{*}, Mahmoud A. A. Abouelatta, Ke Wang Muamer Kadic and Martin Wegener^{*}

E-mail: (yi.chen@partner.kit.edu (Y.C.); martin.wegener@kit.edu (M.W.))

Note 1. Derivation of cable-network band structure

We derive the band structure for finite propagation losses γ of the coaxial cables. To obtain the formula given in the main paper, one can simply set $\gamma = 0$. The case of $\gamma \neq 0$ prepares us for the next section of the Supporting Information.

We consider the model schematically shown in Figure S1 (also see Figure 1 of main paper) for the non-local cable-network metamaterial. The connectors in the cable-network metamaterials are orders of magnitude smaller than the corresponding wavelength. Therefore, we consider them as point-like objects, as indicated by the black dots in Figure 1. The connector at lattice site j is linked to the connectors at the neighboring sites $j + 1$ and $j - 1$ through cables. Furthermore, we introduce N^{th} order interactions through cables that link the connector at site j and the connectors at sites $j - N$ and $j + N$. For the cables mediating the 1st order (local) interactions and the N^{th} order (nonlocal) interactions, we assume the lengths l_1 and l_N , the wave impedances Z_1 and Z_N , and the cable wave speeds c_1 and c_N . All the cables are assumed to have the same loss factor γ as indicated below. The lattice constant or period along the horizontal direction is denoted as a .

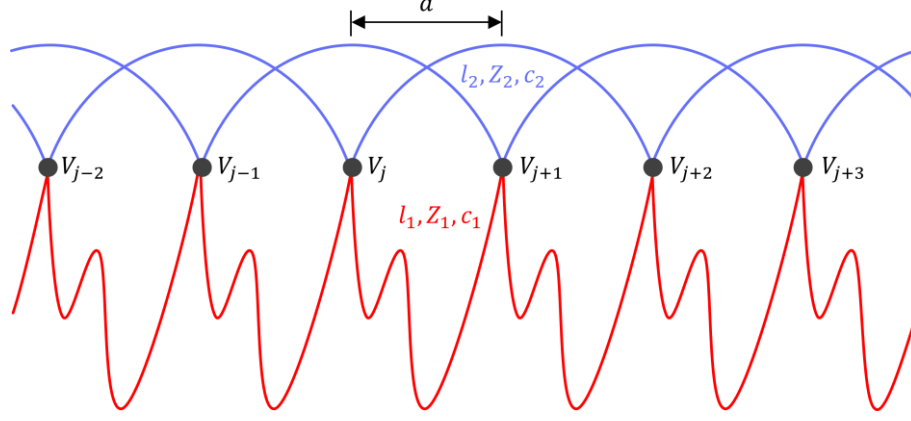


Figure S1. Scheme of the cable-network metamaterials (also see Figure 1). The black dots indicate point-like connectors. Each connector is connected to its immediate neighbor connectors to the left and right at a distance a via cables (red lines) with length l_1 . In addition, each connector is connected to its N^{th} -nearest neighboring connectors to the left and right, respectively, at a distance Na via the cables (blue lines) with length l_N . Here, $N = 2$ serves as an example. Note that the spatial period of the structure is a .

We denote the voltage of the point-like connector at lattice site j as V_j , with $j = -\infty, \dots, -1, 0, +1, \dots, \infty$. We model the wave propagation on an individual cable following transmission line theory.^[1] The voltage distribution along the cable that links the two lattice sites j and site $j + 1$ is given by

$$V_j^{(1)}(s) = A_j^+ \exp(ik_1 s) + A_j^- \exp(-ik_1 s), \quad (\text{S1})$$

with $k_1 = \omega/c_1 + i\gamma$ being the complex wave number. The parameter s represents the propagation coordinate along the cable, with $s = 0$ and $s = l_1$ corresponding to the lattice site j and lattice site $j + 1$, respectively. A_j^+ and A_j^- are the complex amplitudes of the forward and backward propagating waves in the cable. The voltages of the cable ends are equal to the voltages at the point-like connectors. This leads us to

$$V_j^{(1)}(0) = V_j, \quad (\text{S2})$$

$$V_j^{(1)}(l_1) = V_{j+1}. \quad (\text{S3})$$

Furthermore, we have the relation from Bloch's theorem

$$V_{j+1} = V_j \exp(ika), \quad (\text{S4})$$

where k represents the Bloch wave number. From Equation (S2) - (S4), we obtain the two coefficients A_j^+ and A_j^- as

$$A_j^+ = \frac{\exp(ika) - \exp(-ik_1 l_1)}{\exp(ik_1 l_1) - \exp(-ik_1 l_1)} V_j, \quad (\text{S5})$$

$$A_j^- = \frac{\exp(ik_1 l_1) - \exp(ika)}{\exp(ik_1 l_1) - \exp(-ik_1 l_1)} V_j. \quad (\text{S6})$$

Next, the current distribution along the cable that links the sites j and $j + 1$ is obtained from

$$I_j^{(1)}(s) = \frac{1}{Z_1} (A_j^+ \exp(ik_1 s) - A_j^- \exp(-ik_1 s)), \quad (\text{S7})$$

with the complex wave number $k_1 = \omega/c_1 + i\gamma$ and the impedance of the local cables Z_1 as introduced above.

Likewise, we derive the voltage and current distribution along the nonlocal cable that links the connectors at lattice sites j and $j + N$

$$V_j^{(N)}(s) = B_j^+ \exp(ik_N s) + B_j^- \exp(-ik_N s), \quad (\text{S8})$$

$$I_j^{(N)}(s) = \frac{1}{Z_N} (B_j^+ \exp(ik_N s) - B_j^- \exp(-ik_N s)), \quad (\text{S9})$$

$$B_j^+ = \frac{\exp(iNka) - \exp(-ik_N l_N)}{\exp(ik_N l_N) - \exp(-ik_N l_N)} V_j, \quad (\text{S10})$$

$$B_j^- = \frac{\exp(ik_N l_N) - \exp(iNka)}{\exp(ik_N l_N) - \exp(-ik_N l_N)} V_j, \quad (\text{S11})$$

with the complex wave number $k_N = \omega/c_N + i\gamma$ and the wave impedance of the nonlocal cables Z_N as introduced above.

Next, we analyze the current flow to the point-like connector at lattice site j . The current that flows away from the connector at lattice site j to lattice site $j + 1$ is given by $I_j^{(1)}(0)$. The current that flows into the connector at lattice site j from the lattice site $j - 1$ is $I_j^{(1)}(l_1) \exp(-ika)$. The exponential factor $\exp(-ika)$ stems from Bloch's theorem. Likewise, the current that flows away from the connector at lattice site j to the lattice site $j + N$ is given by $I_j^{(N)}(0)$ and the one that flows into the connector at lattice site j from lattice site $j - N$ is given by $I_j^{(N)}(l_N) \exp(-iNka)$. By further applying Kirchhoff's current continuity law to the connector at lattice site j , we obtain

$$I_j^{(1)}(0) - I_j^{(1)}(l_1) \exp(-ika) + I_j^{(N)}(0) - I_j^{(N)}(l_N) \exp(-iNka) = 0. \quad (\text{S12})$$

We note that Kirchhoff's voltage law (energy conservation) is implicitly included in the above assumption for the voltages. From Equation (S12), we obtain the implicit equation for the cable-network metamaterial dispersion relation

$$\frac{\cos(Nka) - \cos(\omega l_N/c_N - i\gamma l_N)}{Z_N \sin(\omega l_N/c_N - i\gamma l_N)} + \frac{\cos(ka) - \cos(\omega l_1/c_1 - i\gamma l_1)}{Z_N \sin(\omega l_1/c_1 - i\gamma l_1)} = 0. \quad (\text{S13})$$

For the case of zero losses, $\gamma = 0$, the dispersion relations $\omega = \omega_i(k)$ with integer band index $i = 1, 2, \dots$ shown in Figure 2 and 3 have been obtained by numerical solution of Equation (S13). The case of $\gamma \neq 0$ is discussed next.

Note 2. Cable-network band structure in the presence of finite losses

In the main paper, we have considered the ideal case of lossless cables. The experiments reported in the main paper come fairly close to this ideal. Nevertheless, it is interesting to ask what the effect of finite losses would be, e.g., due to propagation losses in the coaxial cables. In the preceding section, we have derived the general mathematical background for finite losses, i.e., for $\gamma \neq 0$.

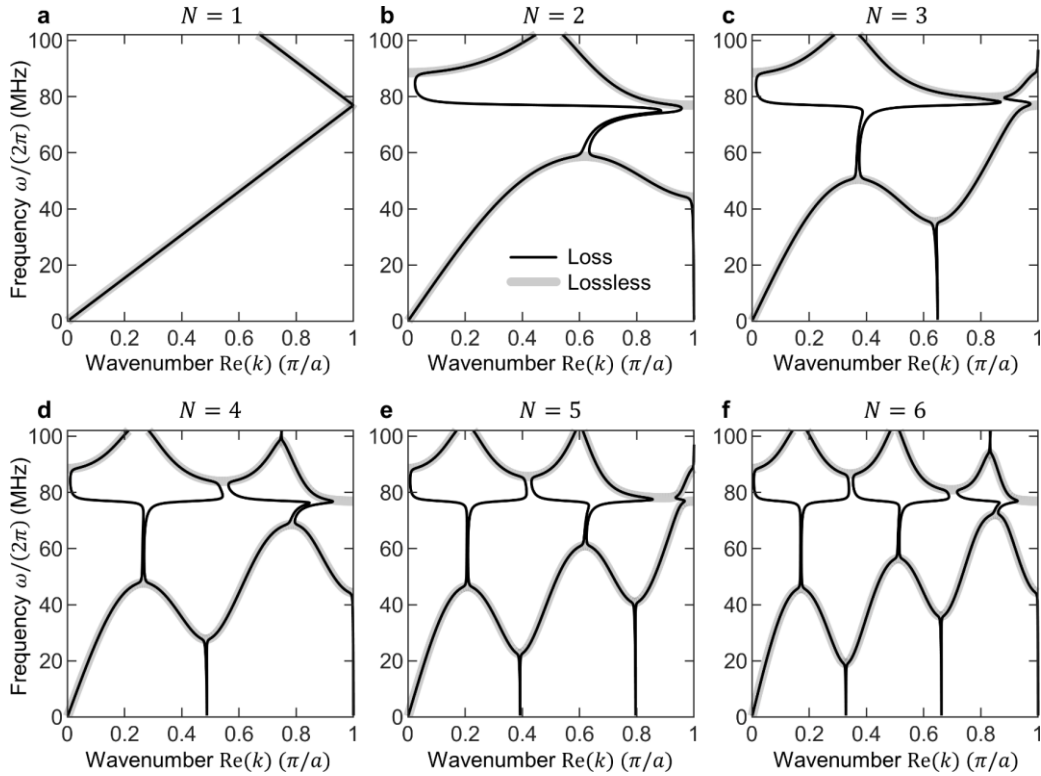


Figure S2. Calculated band structures of the cable-network metamaterial with finite losses. (a) - (f) correspond to $N = 1, 2, 3, 4, 5,$ and 6 . The cable lengths and all other parameters are the same as for Figure 3 in the main paper, but the loss parameters γ in Equation (S13) is not zero and rather chosen to be $\gamma = 0.015 \text{ m}^{-1}$. The black curves are solutions of Equation (S13) for which the frequency is purely real-valued. This frequency is plotted versus the real part of the complex Bloch wavenumber \mathbf{k} . To allow for a direct comparison, the band structure for $\gamma = 0$ is shown by the gray curves (also cf. Figure 3).

In Figure S2, we plot the resulting dispersion relations for the same parameters as in Figure 2 of the main paper, but for a finite loss of $\gamma = 0.015 \text{ m}^{-1}$. This value corresponds to an attenuation of 0.13 dB/m, comparable to losses in common coaxial cables at a frequency of 100 MHz. It becomes obvious that the modifications of the dispersion relation emerge from the maxima and minima of the dispersion relation. This is expected as the extrema are exceptional points.^[2]

Note 3. Obtaining the effective refractive index

In the absence of losses, the refractive index $\tilde{n}(k)$ is real-valued. Its modulus results from the dispersion relation

$$\tilde{n}^2(k) = c^2 \frac{k^2}{\omega_1^2(k)}, \quad (\text{S14})$$

with c being the speed of wave in the coaxial cables. If the phase velocity and the Poynting vector are parallel (antiparallel), the sign of the refractive index is positive (negative). In the absence of losses, the Poynting vector and the group-velocity vector point in the same direction. Therefore, for our conditions, the sign of the refractive index is identical to the sign of the slope $d\omega/dk$ in the dispersion relations $\omega(k)$ shown in Figure 3. From parametrically plotting $\omega_1(k)$ on the horizontal axis and $\tilde{n}(k)$ for positive k on the vertical axis of a figure, one gets the dependence of the refractive index on frequency, $n(\omega) = \tilde{n}(k(\omega))$, which is multi-valued as illustrated in Figure 4 of the main paper for the same examples as in Figure 3. In particular, it contains broad regions of negative refractive index – conceptually at zero loss. We emphasize that the frequency dependence of the refractive index in Figure 4, which is due to nonlocal interactions, is qualitatively distinct from that one gets for local resonances.

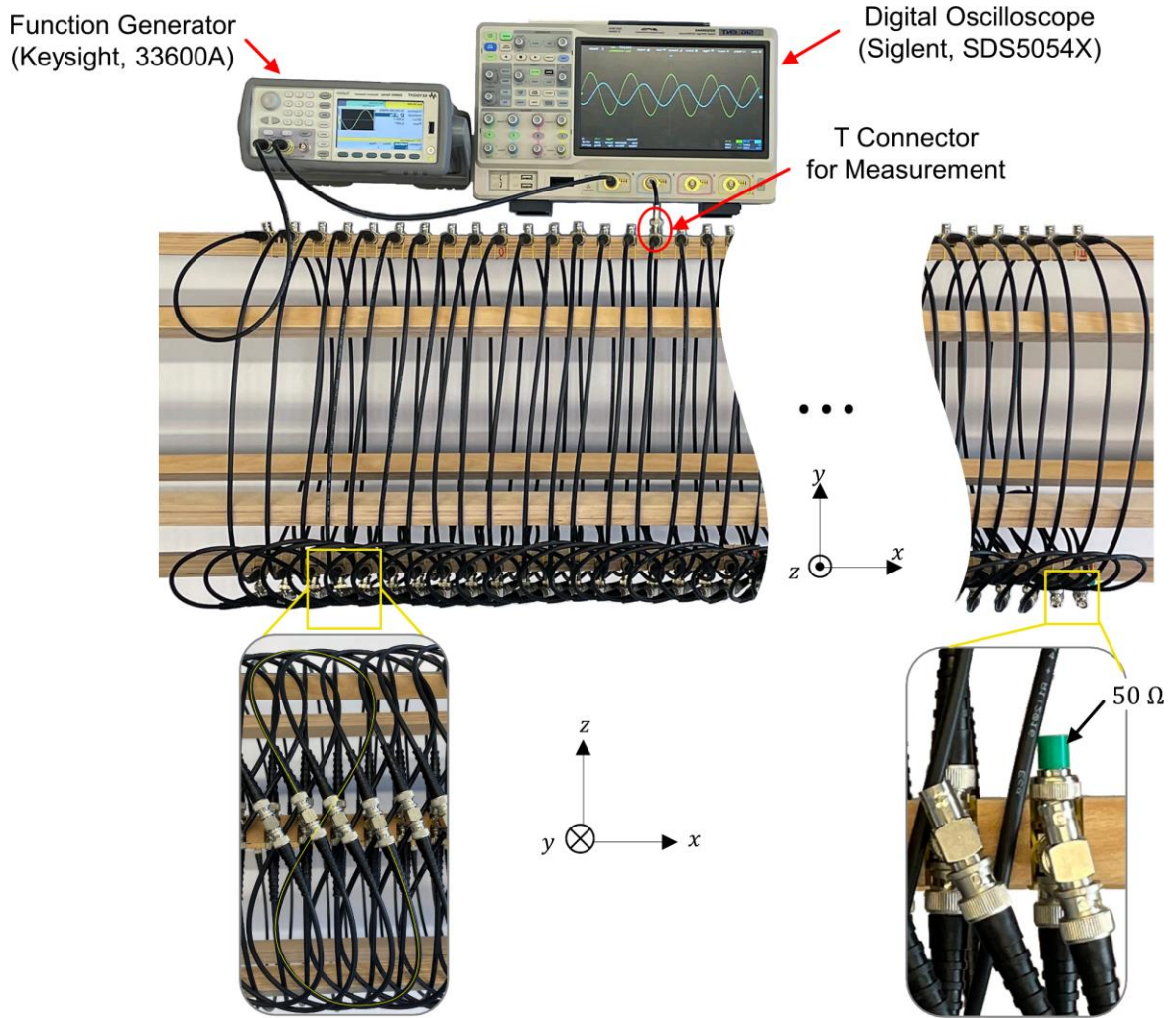


Figure S3. Photograph of experiment setup. The left-hand side of the metamaterial is connected to a function generator and its right-hand side end is terminated by a 50Ω resistor (see lower right-hand side inset). During the experiment, we measure the voltages at the top BNC T-connectors (also cf. Figure 1) by successively connecting them to a digital oscilloscope via a 10 cm short cable. Furthermore, we connect another channel of the digital oscilloscope directly to the function generator to synchronize the measurement while taking data at the different T-connectors. A cable-network metamaterial with $N = 2$ (see the yellow line in lower left-hand side inset) is used as an example here, as in Figure 1 of the main paper.

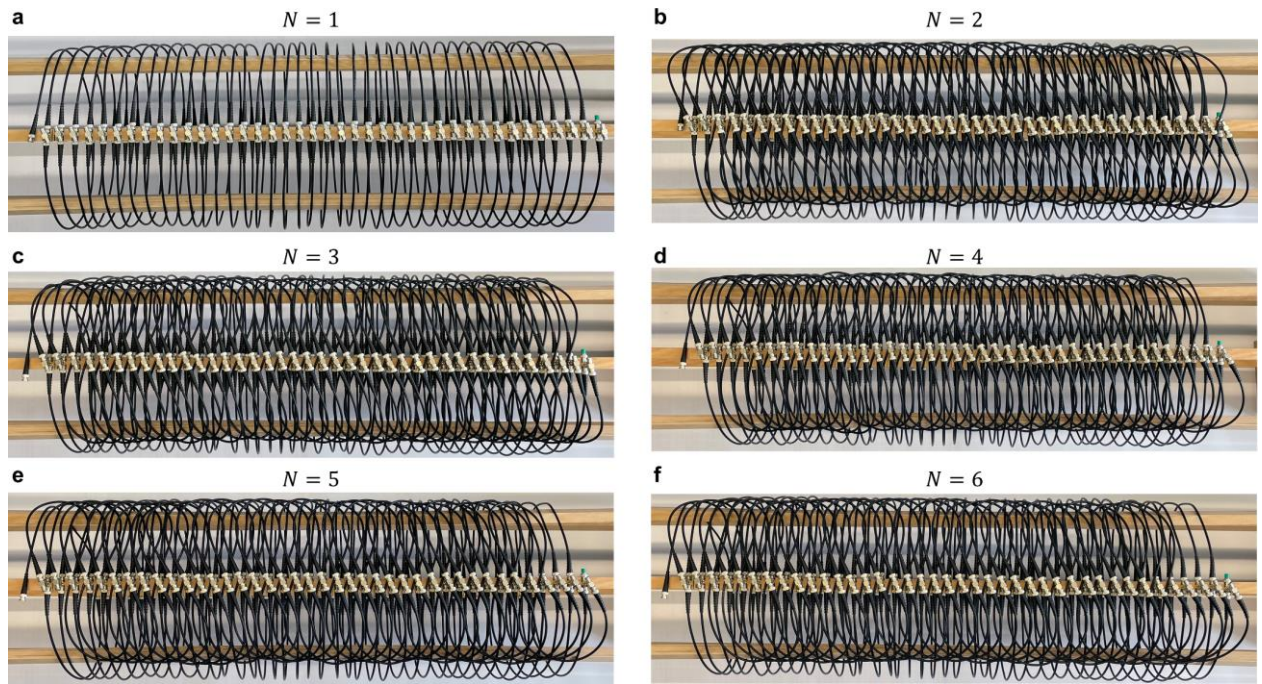


Figure S4. Photographs of considered metamaterials. (a) - (f) correspond to $N = 1, 2, 3, 4, 5,$ and 6 (also cf. Figure S3). Band structures measured on these six samples are depicted in Figure 3 of the main paper.

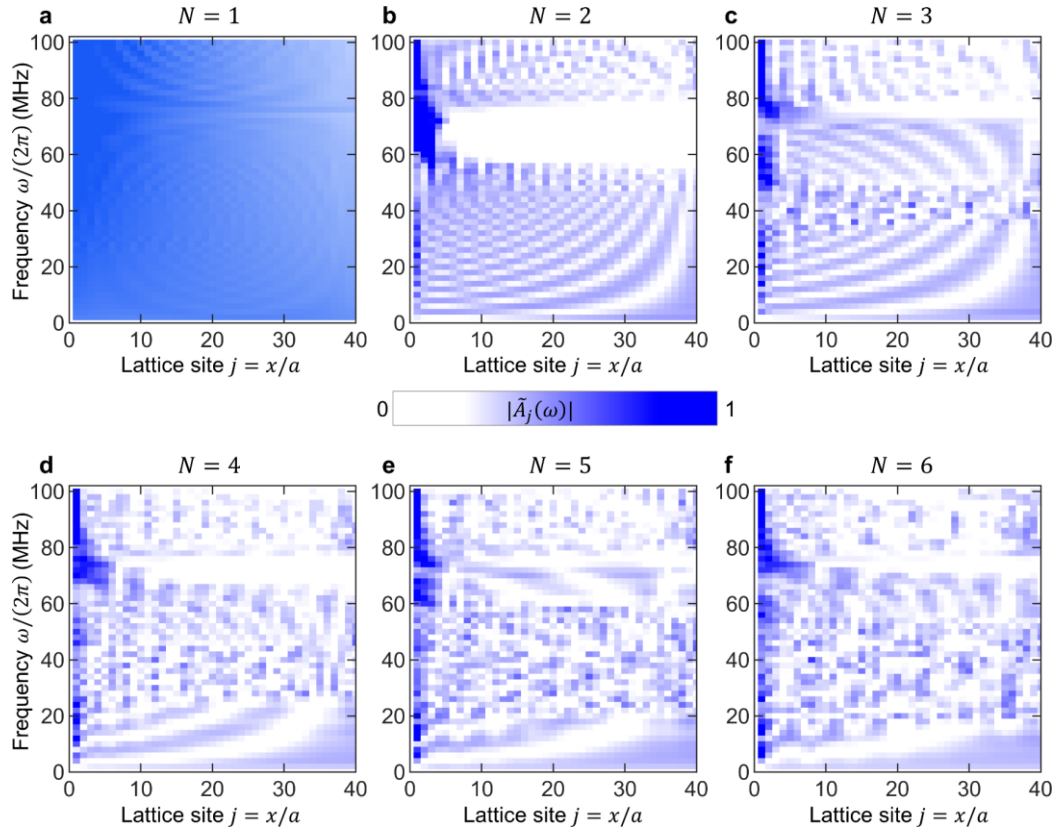


Figure S5. Real-space raw data corresponding to the band structures shown in Figure 3. (a) - (f) Measured voltage amplitude versus lattice site $j = x/a$ and frequency for $N = 1, 2, 3, 4, 5,$ and 6 . The dispersion relations shown in Figure 3 have been derived by a spatial Fourier transformation of these real-space data.

References:

- [1] T. Itoh, C. Caloz, *Electromagnetic metamaterials: transmission line theory and microwave applications*, John Wiley, New York **2005**.
- [2] M. A. Miri, A. Alu, *Science* **2019**, 363, 7709.